Current-phase relation and h/e-periodic critical current of a chiral Josephson contact between one-dimensional Majorana modes

Dmitriy S. Shapiro,[1,2,3,*] Alexander Shnirman,[4] and Alexander D. Mirlin[1,4,5]

[1]*Institut für Nanotechnologie, Karlsruhe Institute of Technology, Karlsruhe 76021, Germany*
[2]*V. A. Kotel'nikov Institute of Radio Engineering and Electronics, Russian Academy of Sciences, Moscow 125009, Russia*
[3]*Dukhov Research Institute of Automatics (VNIIA), Moscow 127055, Russia*
[4]*Institut für Theorie der Kondensierten Materie, Karlsruhe Institute of Technology, Karlsruhe 76128, Germany*
[5]*Petersburg Nuclear Physics Institute, St. Petersburg 188300, Russia*

We explore a long Josephson contact transporting Cooper pairs between one-dimensional (1D) charge-neutral chiral Majorana modes in the leads via charged Dirac chiral modes in the normal region. We investigate the regimes of (i) transparent contacts and (ii) tunnel junctions implemented in 3D topological insulator/superconductor/magnet hybrid structures. The setup acts as a SQUID controlled by the magnetic flux enclosed by the chiral loop of the normal region. This chirality leads to the fractional h/e-periodic pattern of critical current. The current-phase relation can have sawtoothlike shape with spikes at unusual even phases of $2\pi n$.

I. INTRODUCTION

Intensive studies of Majorana fermion physics in solid state materials were motivated by possible applications of these states in topological quantum computation [1,2]. In condensed matter, initially, Majorana fermions were predicted to exist in spinless p-wave superconductors (SC) and fractional QHE [3–5]. Later, the realizations of Majorana bound states (MBS) [6–8] and one-dimensional (1D) charge-neutral modes [9] were proposed in hybrid structures where a helical electronic system has a proximity effect with external s-wave pairing potential and Zeeman exchange field. The helical systems with spin and momentum locking are realized in surfaces and edges of topological insulators (TI), quantum spin-Hall films [10], and semiconductors with strong spin-orbital coupling [7,11]. The transport signatures of MBS are associated with anomalous 4π-periodic Josephson effect [3,6,12,13]. On the other hand, charge-neutral chiral Majorana modes (χMM) which are, for instance, supported by SC-magnet junctions on 3D TI surface [9,14], are expected to show unconventional interferometry if involved in charge transfer between normal metal leads. Various χMM-based devices operating as Mach-Zehnder [14,15], Fabry-Pérot [16,17], and Hanbury-Brown Twiss [18] quantum interferometers have been proposed. In the context of quantum computation they can serve as a readout tool of qubit states encoded by MBS in vortex cores [15].

In the paper we calculate DC Josephson current-phase relation (CΦR) of a long spinless contact between 1D gapless χMMs. The system under consideration represents a chiral Fabry-Pérot interferometer implemented on a surface of 3D TI partially gapped by SC and magnetic (M) islands. Similar ideas were explored in Refs. [14–18]. In these works normal dissipative transport of Dirac fermions influenced by their splitting to Majorana modes and the interference of the latter were studied. In contrast, we study the equilibrium phenomenon of Josephson current carried by the Andreev

states formed in the chiral Dirac liquid. The latter connects between two superconducting leads, which are effectively gapless due to chiral Majorana modes at their edges. Spinless structure of the junction follows from the absence of spin degeneracy of 2D helical surface states. Presence of Zeeman field breaks time-reversal symmetry and produces gapless chiral channels at the magnetic domain boundaries. In our system the normal conducting region consists of two separated chiral Dirac channels supported by magnetic domain walls.

We explore two models of (i) transparent and (ii) tunnel junctions. The first one involves four chiral Y junctions, operating as direct charged-to-neutral fermion converters. The second one has two tunnel contacts formed by thin layers of magnetic material where Majorana and normal Dirac channels are hybridized. The length of the N region, formed by two counterpropagating 1D Dirac modes, is assumed to be larger than coherence length of the induced superconductivity. In other words, the Thouless energy of the normal conducting part of the system under consideration is significantly smaller than the proximity gap.

We take into account a contribution to the transport from subgap 1D chiral states only, neglecting 2D bands. Since our superconducting leads are gapless due to the presence of χMMs, the spectral current is continuous and consists of smeared Andreev levels. Assuming that superconducting leads are large and have a fixed chemical potential, we obtain the conventional 2π periodicity of the CΦR. In other words, the nonequilibrium 4π-periodic Josephson effect (which is predicted [19] for systems with zero-energy MBSs) turns out to be irrelevant here.

The chiral structure of the normal part consisting of two 1D spinless Dirac modes allows one to make Andreev pairs nonlocal. This means that the pair resides on two separated Dirac channels and one can apply magnetic flux f inducing Aharonov-Bohm phase $\phi_{AB} = 2\pi f/(h/e) = \pi f/\Phi_0$, where $\Phi_0 = h/(2e)$. It follows that the critical current has a $2\Phi_0$ periodicity rather than the conventional Φ_0 one. The spatial separation of the Andreev pairs distinguishes our setup from the junctions with 2D topological insulators sandwiched

*shapiro@cplire.ru

between superconducting leads, where Andreev pairs propagate on the same edge [20,21]. Setups with spatially separated Andreev pairs based on the quantum Hall chiral edges were analyzed in Refs. [22,23]. In Sec. VI we compare those systems with ours.

The paper is organized as follows. In Sec. II we present the main ideas of χMMs realization in hybrid structures on a surface of 3D topological insulator. In Sec. III we consider the regime of transparent Josephson contacts. We derive the S matrix of the contacts by means of matching the field operators in the chiral channels. Next we calculate Josephson CΦR at arbitrary temperature and flux enclosed by Dirac modes. Section IV addresses the tunneling regime, in which Majorana and Dirac modes meet at the tunnel contacts formed by magnetic constrictions. In Sec. V we discuss the Majorana representation of charged-to-neutral fermion scattering in transparent and tunnel contacts. Section VI summarizes the results of this paper. The technical details are provided in Appendixes A and B.

II. MAJORANA MODES IN 3D TI HYBRID STRUCTURE

As was proposed by Fu and Kane [6], the χMM is supported by SC/magnet/3D-TI structure like that shown in Fig. 1, with an effective low-energy 1D Hamiltonian following from a solution of a 2D Bogolyubov–de Gennes equation. The 2D surface states are described by the Rashba Hamiltonian. The system is assumed to have a chemical potential $\mu = 0$, corresponding to the Dirac point. The induced s-wave SC pairing potential is given by $\Delta e^{i\Phi_{SC}}$ in the $y < 0$ half plane, while at $y > 0$ there is magnetic material inducing Zeeman exchange field $M\sigma_z$. The full Hamiltonian reads

$$
\begin{aligned}
H &= \frac{1}{2} \int dx\, dy\, \Psi^+ h \Psi, \\
h &= iv\tau_z \mathbf{z} \cdot (\boldsymbol{\sigma} \times \boldsymbol{\nabla}) - M\theta(y)\sigma_z \\
&\quad + (\tau_+ \Delta e^{-i\Phi_{SC}} + \tau_- \Delta e^{i\Phi_{SC}})\theta(-y),
\end{aligned}
\tag{1}
$$

where the field operator of the 2D surface is $\Psi = [\psi_\uparrow, \psi_\downarrow, \psi_\downarrow^+, -\psi_\uparrow^+]^T$, and $\boldsymbol{\sigma}$ and $\boldsymbol{\tau}$ are Pauli matrices in spin and Nambu spaces, respectively. The field Ψ satisfies the charge conjugation constraint $\Psi = \sigma_y \tau_y \Psi^*$, while the eigenstates obey $\xi_p = \sigma_y \tau_y \xi_{-p}^*$. The low-energy $|\varepsilon_p| < \Delta, M$ eigenvalues of the Bogolyubov–de Gennes equation $h\xi_p = \varepsilon_p \xi_p$ are single degenerate and correspond to a 1D chiral mode
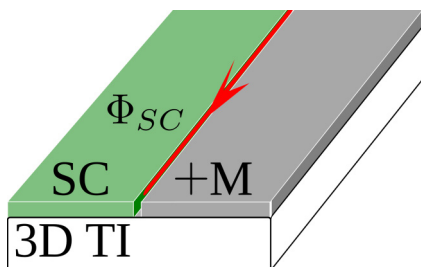

FIG. 1. Superconductor/magnetic insulator boundary on the surface of 3D topological insulator. The boundary supports a chiral Majorana mode with the chirality depending on the sign of the magnetization.

with the linear spectrum

$$
\varepsilon_p = \mathrm{sgn}(M)vp.
\tag{2}
$$

Single degeneracy of eigenvalues implies that Bogolyubov quasiparticle operator

$$
\chi_p = \int dx\, dy \big(\xi_p^{(M)}\big)^\dagger (x,y) \cdot \Psi(x,y)
\tag{3}
$$

represents a Majorana mode obeying $\chi_p = \chi_{-p}^+$. The corresponding wave function of the χMM reads

$$
\xi_p^{(M)}(x,y) = \frac{1}{2}\, g^{(M)}(y)
\begin{bmatrix}
e^{i(\frac{\pi}{4} - \frac{\Phi_{SC}}{2})} \\
-\mathrm{sgn}(M)e^{-i(\frac{\Phi_{SC}}{2} + \frac{\pi}{4})} \\
-\mathrm{sgn}(M)e^{i(\frac{\Phi_{SC}}{2} + \frac{\pi}{4})} \\
-e^{i(\frac{\Phi_{SC}}{2} - \frac{\pi}{4})}
\end{bmatrix}
e^{ipx}.
\tag{4}
$$

The momentum p here is directed along x axis and $g^{(M)}(y) = e^{y(l_{sc}^{-1}\theta(-y) - l_m^{-1}\theta(y))}/\sqrt{2(l_{sc} + l_m)}$ is the transverse shape of 1D guiding channel. The coherence lengths (transversal decay lengths) are given by $l_{sc} = \hbar v/\Delta$ and $l_m = \hbar v/M$. The superscript (M) in Eqs. (3) and (4) emphasizes the Majorana nature of the mode.

Another building block of chiral interferometers is a domain wall on a surface of a 3D TI where the magnetization sign is changed. If we consider such a $-$M/+M boundary along the x axis, which is described by the term $M\sigma_z \mathrm{sgn}(y)$ in the Bogolyubov–de Gennes Hamiltonian, we end up with the Dirac chiral mode with the same spectrum found for χMM (2). In the Nambu notation any of ε eigenvalues are doubly degenerate and related to orthogonal electron and hole eigenstates $\xi_p^{(e)}$ and $\xi_p^{(h)} = \sigma_y \tau_y \xi_{-p}^{(e)*}$, where

$$
\xi_p^{(e)}(x,y) = \frac{1}{\sqrt{2}}\, g^{(D)}
\begin{bmatrix}
1 \\
i\,\mathrm{sgn}(M) \\
0 \\
0
\end{bmatrix}
e^{ipx}
\tag{5}
$$

and $g^{(D)} = \exp(-|y|/l_m)/\sqrt{2l_m}$. There are two independent excitations with energy ε in Nambu notation in this $-$M/+M case—the electron with momentum p and Bogolyubov operator ψ_p and the $-p$ hole with ψ_{-p}^+. This field is complex $\psi_p \neq \psi_{-p}^+$ and corresponds to a charged mode. We introduce here 1D operators $\psi(x), \chi(x)$

$$
\chi(x) = \chi^+(x) = \int \frac{dp}{2\pi} \chi_p e^{-ipx}, \quad \psi(x) = \int \frac{dp}{2\pi} \psi_p e^{-ipx},
$$

with the anticommutation rules given by

$$
\begin{aligned}
\{\psi^+(x_1), \psi(x_2)\} &= \delta(x_1 - x_2), \\
\{\psi(x_1), \psi(x_2)\} &= 0, \\
\{\chi(x_1), \chi(x_2)\} &= \delta(x_1 - x_2).
\end{aligned}
$$

The same relations hold in the Heisenberg picture at equal times $t_1 = t_2$. After that the secondary quantized operators in the low energy range $|\varepsilon| < \Delta, M$ can be found as sums over subgap chiral states. For the charge-neutral Majorana excitations we obtain

$$
\Psi_M(x,y) = \int \frac{dp}{2\pi} \xi_p^{(M)}(x,y) \chi_p,
$$

while for the Dirac mode the field reads

$$\Psi_D(x,y) = \int \frac{dp}{2\pi} (\xi_p^{(e)}(x,y)\psi_p + \xi_p^{(h)}(x,y)\psi_{-p}^+).$$

Substituting these fields into the second quantized Bogolyubov–de Gennes Hamiltonian and performing the transverse integration we obtain the following 1D Hamiltonians:

$$H_M = \mathrm{sgn}(M)\frac{iv}{2} \int dx\, \chi(x)\partial_x \chi(x) \tag{6}$$

and

$$H_D = \mathrm{sgn}(M)iv \int dx\, \psi^+(x)\partial_x \psi(x). \tag{7}$$

The Hamiltonians (6) and (7) correspond to coherent propagation of the excitations in 1D guiding channels with the Fermi velocity v and chirality dependent on the sign of the magnetization. The $1/2$ in the Majorana Hamiltonian H_M reflects the fact that independent excitations in the χMM can be considered either at positive or negative energies only. Say, the bottom branch of the chiral mode (2) at $p < 0$ is redundant.

The wave functions $\xi^{(M)}$ or $\xi^{(e)}$ show that the spin direction is locked to the momentum. More specifically, the spin textures of the guiding channels of Majorana and Dirac modes are orthogonal to the momentum direction in the particular case of Rashba type Hamiltonian (1). As a consequence the spin textures are antiparallel in the counterpropagating channels. More generally, any scattering at a junction will be accompanied by the corresponding spin rotation.

III. TRANSPARENT REGIME

A. S matrix of a transparent contact

In this section we consider the Josephson junction shown in Fig. 2. This consists of two counterpropagating chiral Dirac modes which scatter at the left and right contacts with the superconducting leads. Each of these contacts consists of a pair of chiral Y junctions where electrons convert into a pair of Majorana fermions with opposite chiralities or vice versa (see Fig. 3). The full S matrix of this contact is derived from two operator relations for both upper and lower Y
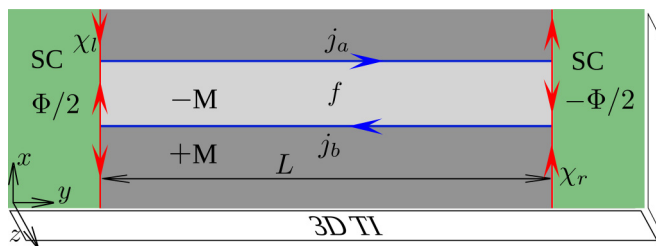

FIG. 2. Scheme of transparent Josephson junction on the surface of 3D topological insulator. Red lines stand for gapless Majorana fermion channels and arrows reflect chiralities. Superconducting electrodes, marked as green, have phase difference Φ. Light and dark gray bars are magnetic materials which induce exchange fields of the opposite polarizations $\pm M$. The line of the sign change of M supports chiral charged modes marked as blue. Magnetic flux f in $-M$ region induces Aharonov-Bohm phase $\phi_{AB} = \pi f/\Phi_0$.
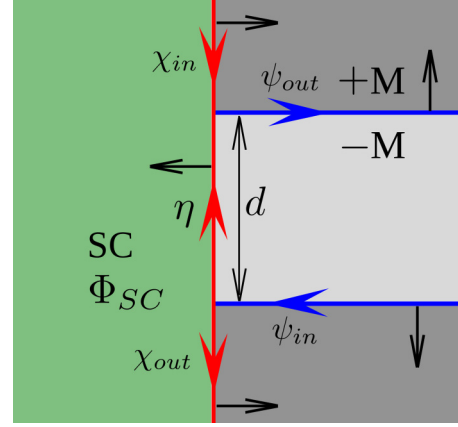

FIG. 3. Structure of the contact. Black arrows shows spin texture of the chiral modes.

junctions, described by S_{out} and S_{in} matrices found in Refs. [14,15]. Let us assume first that $\Phi_{\mathrm{SC}} = 0$ in the electrode. The matrix S_{in} involves phase difference between electron and hole converting into two Majorana fermions. This phase is denoted as α and is included in the scattering matrix as follows:

$$\begin{bmatrix} \eta_{\mathrm{out}} \\ \chi_{\mathrm{out}} \end{bmatrix} = S_{\mathrm{in}} \begin{bmatrix} \psi_{\mathrm{in}} \\ \psi_{\mathrm{in}}^+ \end{bmatrix}, \tag{8}$$

$$S_{\mathrm{in}} = \begin{bmatrix} 1/\sqrt{2} & 1/\sqrt{2} \\ i/\sqrt{2} & -i/\sqrt{2} \end{bmatrix} \begin{bmatrix} e^{i\alpha} & 0 \\ 0 & e^{-i\alpha} \end{bmatrix}. \tag{9}$$

The fields entering Eq. (8) are Heisenberg operators at a given energy. The S_{out} matrix was found in Ref. [15] by means of time reversal transformation of S_{in} which changes the magnetization sign $M \to -M$

$$S_{\mathrm{out}}(M) = S_{\mathrm{in}}^T(-M). \tag{10}$$

We assume here that both Y junctions have identical geometries (and, in particular, α is the same). In this work we set the value of α as a free parameter which is to be found from a particular geometry of the Y junction. The scattering in the upper Y junction in Fig. 3 reads as

$$\begin{bmatrix} \psi_{\mathrm{in}} \\ \psi_{\mathrm{in}}^+ \end{bmatrix} = S_{\mathrm{out}} \begin{bmatrix} \eta_{\mathrm{in}} \\ \chi_{\mathrm{in}} \end{bmatrix}. \tag{11}$$

We match Majorana operators η_{in} and η_{out} for the given energy ε as $\eta_{\mathrm{in},\varepsilon} = e^{ik_\varepsilon}\eta_{\mathrm{out},\varepsilon}$, where the dynamic phase $k_\varepsilon = \varepsilon d/v$ is accumulated by the Majorana excitation in course of the propagation from the lower to the upper Y junction separated by the distance d. The full $S(\Phi_{\mathrm{SC}}{=}0)$ matrix of the left contact is found straightforwardly after the exclusion of η fields from Eqs. (9), (10) and their Hermitian conjugates. To reinstate a nonzero SC phase of the electrode Φ_{SC} (colored as green in Fig. 3), we employ the transformation $\psi \to e^{i\Phi_{\mathrm{SC}}/2}\psi$, yielding

$$S = \begin{bmatrix} \frac{1}{2}e^{i(k_\varepsilon+2\alpha)} & \frac{i}{\sqrt{2}}e^{i\frac{2\alpha-\Phi_{\mathrm{SC}}}{2}} & \frac{1}{2}e^{i(k_\varepsilon-\Phi_{\mathrm{SC}})} \\ \frac{i}{\sqrt{2}}e^{i\frac{2\alpha+\Phi_{\mathrm{SC}}}{2}} & 0 & \frac{-i}{\sqrt{2}}e^{-i\frac{2\alpha+\Phi_{\mathrm{SC}}}{2}} \\ \frac{1}{2}e^{i(k_\varepsilon+\Phi_{\mathrm{SC}})} & \frac{-i}{\sqrt{2}}e^{i\frac{\Phi_{\mathrm{SC}}-2\alpha}{2}} & \frac{1}{2}e^{i(k_\varepsilon-2\alpha)} \end{bmatrix}. \tag{12}$$

This unitary S matrix has particle-hole symmetry

$$S(\varepsilon) = \mathcal{Z} S^*(-\varepsilon) \mathcal{Z}, \quad \mathcal{Z} = \begin{bmatrix} 0 & 0 & 1 \\ 0 & 1 & 0 \\ 1 & 0 & 0 \end{bmatrix}$$

and acts on $(\psi_{\text{in},\varepsilon}, \chi_{\text{in},\varepsilon}, \psi_{\text{in},-\varepsilon}^+)^T$. It describes the partial Andreev reflection in spinless Dirac channel, which is combined with neutral Majorana excitations. The Andreev part of this process is accompanied by a Cooper pair absorption by the SC electrode.

B. Current-phase relation of transparent junction

In the following consideration we assume that chiral Dirac channels have equal lengths, are parallel to each other, and separated by the distance d. Using the above approach based on S-matrix (12), we find ψ operators of charged fermions as linear combinations of uncorrelated field operators χ_l and χ_r of incident Majorana modes. The latter are characterized by the Fermi distribution function:

$$\langle \chi_{\varepsilon,i}^{\dagger} \chi_{\varepsilon,j} \rangle = \frac{v^{-1} \delta_{i,j}}{1 + e^{\varepsilon/T}}, \quad \chi_\varepsilon = \chi_{-\varepsilon}^{\dagger} = \int \chi(t) e^{i\varepsilon t} dt, \quad (13)$$

where v^{-1} is the density of states in the χ MM channels. We assume $k_B = 1$ everywhere and recover it in final expressions. Using operator relations, we calculate chiral local densities of states $\rho_\varepsilon^{(a)}, \rho_\varepsilon^{(b)}$ and currents j_a, j_b. The linear spectrum of the system (2) means that chiral current j_i is proportional to

charge density and, hence, the Josephson current j is given by

$$j = j_a - j_b = -ev(\langle \psi_a^+ \psi_a \rangle - \langle \psi_b^+ \psi_b \rangle). \quad (14)$$

The positive direction of the current is defined from left to right SC, bias voltage is zero, and the SC phases on the electrodes are equal to $\pm \Phi/2$, as shown in Fig. 2. While solving for Dirac $\psi_{\varepsilon,i}$ operators, we take into account the dynamic φ_ε and the Aharonov-Bohm ϕ_{AB} phases

$$\varphi_\varepsilon = \frac{\varepsilon}{E_T}, \quad \phi_{AB} = \pi \frac{f}{\Phi_0}.$$

The Thouless energy E_T here is equal to inverse dwell time of the interferometer (or the level spacing in the N region)

$$E_T = \frac{\hbar v}{2L + 2d}. \quad (15)$$

Dynamic phase φ_ε is accumulated by ε electron or $-\varepsilon$ hole enclosing the interference loop of total length $2L + 2d$. Calculations of expressions for $\psi_{\varepsilon,i}$ are analogous to those presented in Appendix B for tunnel junction.

Within this S-matrix formalism, valid for energies in the range $|\varepsilon| < \Delta, M$, we find the following result for the CΦR:

$$j(\Phi, \phi_{AB}) = \frac{e}{\hbar} \int J_\varepsilon(\Phi, \phi_{AB}) n_F(\varepsilon, T) d\varepsilon, \quad (16)$$

where the distribution function is determined by that of the incoming χ MMs defined in (13). The spectral current J_ε can be associated with the local densities of states in the arms a, b via $J_\varepsilon = ev(\rho_\varepsilon^{(a)} - \rho_\varepsilon^{(b)})$. The densities of states $\rho_\varepsilon^{(a)}$, discussed in Sec. IV C 2, have dimension of inverse velocity; hence J_ε is dimensionless. We obtain

$$J_\varepsilon(\Phi, \phi_{AB}) = \frac{-\sin \varphi_\varepsilon \sin \Phi}{1 + \left(\frac{\cos(\phi_{AB} + 4\alpha) + \cos \Phi}{2} \right)^2 - (\cos(\phi_{AB} + 4\alpha) + \cos \Phi) \cos \varphi_\varepsilon}. \quad (17)$$

This is a nonsingular 2π-periodic function which reflects the structure of the broadened Andreev levels. As we mentioned in the Introduction, conventional 2π periodicity with respect to Φ is related to the assumption of equilibrium (no transport voltage). This means that there are no parity effects resulting in anomalous 4π Josephson effect.

The integration in Eq. (16) is reduced to a sum over positive Matsubara fermionic frequencies $iT(2\pi n + \pi)$. We note that the dynamical phase takes the values $\varphi_\varepsilon \to iT(2\pi n + \pi)/E_T$ at these Matsubara frequencies. Evaluating the sum, we obtain the CΦR

$$j(\Phi, \phi_{AB}) = 4\pi \frac{e k_B T}{\hbar} \sin \Phi$$

$$\times \sum_{n=0}^{\infty} \frac{1}{2 e^{\pi \frac{k_B T(1+2n)}{E_T}} - \cos(\phi_{AB} + 4\alpha) - \cos \Phi}. \quad (18)$$

This is one of the central results of this paper. It describes the DC Josephson current at arbitrary temperature and takes into account contributions from the subgap 1D states.

At zero temperature the summation in $j(\Phi, \phi_{AB})$ is replaced by an integration over $x = \frac{2\pi T n}{E_T}$ and the result reads

$$j_{T=0}(\Phi, \phi_{AB}) = -2 \frac{e}{\hbar} E_T \frac{\ln \left(1 - \frac{\cos(\phi_{AB} + 4\alpha) + \cos \Phi}{2} \right)}{\cos(\phi_{AB} + 4\alpha) + \cos \Phi} \sin \Phi. \quad (19)$$

The CΦR at zero temperature T is presented in Fig. 4 for the value of the Aharonov-Bohm phase chosen as $\phi_{AB} = -4\alpha$. At this value the first Φ derivative of the current is divergent as $\propto \ln |\Phi|$ at $\Phi \to 0$. This divergence illustrates the tendency of the CΦR to have spikes at even phases $\Phi = 2\pi n$. In Sec. IV C we discuss the limit of full Andreev reflection, where the CΦR has a sawtooth form, also with spikes at $\Phi = 2\pi n$.

Two separated Dirac modes connecting the two superconductors form a SQUID loop. In view of the chirality of the junction the Andreev pair belongs to both Dirac channels, since a reflection into the same channel is forbidden. Considering the junction as a SQUID loop controlled by a magnetic flux applied to the $-M$ light gray bar in Fig. 2, we observe the fractional $2\Phi_0 = h/e$-periodic pattern for the critical current. In Fig. 5 we plot the critical current as a function of the flux-induced Aharonov-Bohm phase $\phi_{AB} = \pi f/\Phi_0$. The
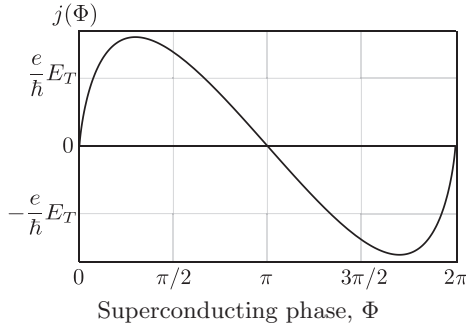
FIG. 4. $T = 0$ CΦR of the transparent junction at $\phi_{AB} = \pi$. Divergent Φ derivatives at $\Phi \to 2\pi n$ are observed.

curve is symmetric under the assumption that $4\alpha = \pi$. (We recall that α is related to the geometry of the Y junctions.) The critical current j_c in this plot is normalized by its maximal value $j_{c,\text{max}}$. At arbitrary α the curve in Fig. 5 would be horizontally shifted. The positions of the peaks of j_c are given by $\phi_{AB,\text{max}} = -4\alpha + 2\pi n$.

IV. TUNNELING REGIME

A. Scattering matrix of a tunnel contact

The realization of the tunneling regime of the Josephson junction studied in this paper is presented in Fig. 6. The left and the right tunnel contacts are implemented as constrictions of the magnetic material (see Fig. 7). Similar to the previous Sec. III, the Dirac channels a and b are colored as blue lines and have equal lengths $l_a = l_b = L$ and geometries. In contrast to the transparent regime, in the tunneling regime the Dirac mode is not terminated but rather forms a closed loop. Hence we introduce the total phase acquired over the loop a sum of the Berry phase π and the Aharonov-Bohm phase, $\phi_{\text{ext}} \equiv \pi + \pi f/\Phi_0$. The constriction of the $+$M magnet plays the role of an insulating barrier.
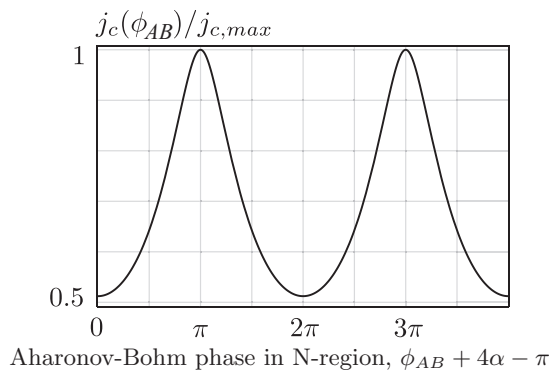

FIG. 5. Fractional h/e-periodic pattern of critical current $j_c(\phi_{AB})$ at $T = 0$. The critical current $j_c(\phi_{AB})$ is normalized to the maximal value $j_{c,\text{max}}$ and plotted as a function of Aharonov-Bohm phase $\phi_{AB} = \pi f/\Phi_0$, where f is the magnetic flux.
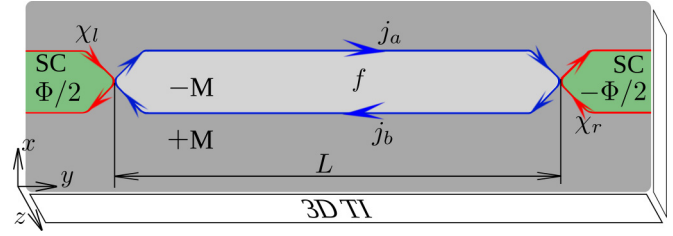

FIG. 6. Scheme of the Josephson junction in the tunneling regime.

We employ the effective 1D Hamiltonians (6), (7) and add a local tunneling term. The resulting Hamiltonian reads

$$H = iv \int \psi^+ \partial_x \psi \, dx - \frac{iv}{2} \int \chi \partial_x \chi \, dx$$
$$+ t\chi \left(\psi \, e^{i\frac{\Phi_{\text{SC}}}{2}} - \psi^+ e^{-i\frac{\Phi_{\text{SC}}}{2}} \right). \quad (20)$$

This Hamiltonian describes counterpropagating Majorana and Dirac modes which mix at $x = 0$. The microscopic structure of the contact is accounted for by the small tunneling amplitude $t \ll v$, which is an additional parameter of our theory.

In Appendix A, using Hamiltonian (20), we derive the scattering matrix S_t of the tunnel contact acting on fields $(\psi_{\text{in},\varepsilon}, \chi_{\text{in},\varepsilon}, \psi^+_{\text{in},-\varepsilon})^T$. The scattering matrix reads

$$S_t = \begin{bmatrix} \frac{1}{1+\lambda} & \frac{i\sqrt{2\lambda}}{1+\lambda} e^{-i\frac{\Phi_{\text{SC}}}{2}} & \frac{\lambda}{1+\lambda} e^{-i\Phi_{\text{SC}}} \\ \frac{i\sqrt{2\lambda}}{1+\lambda} e^{i\frac{\Phi_{\text{SC}}}{2}} & \frac{1-\lambda}{1+\lambda} & \frac{-i\sqrt{2\lambda}}{1+\lambda} e^{-i\frac{\Phi_{\text{SC}}}{2}} \\ \frac{\lambda}{1+\lambda} e^{i\Phi_{\text{SC}}} & \frac{-i\sqrt{2\lambda}}{1+\lambda} e^{i\frac{\Phi_{\text{SC}}}{2}} & \frac{1}{1+\lambda} \end{bmatrix}. \quad (21)$$

The formal solution (21) obtained in Appendix A is valid for any value of t and the dimensionless parameter λ characterizing the scattering is given by

$$\lambda(t) = \tan^2 \frac{t}{\sqrt{2}v}. \quad (22)$$

Yet, since the Hamiltonian (20) is physically justified only in the weak tunneling limit $t \ll v$, we obtain $\lambda \approx (1/2)\,t^2/v^2 \ll 1$.
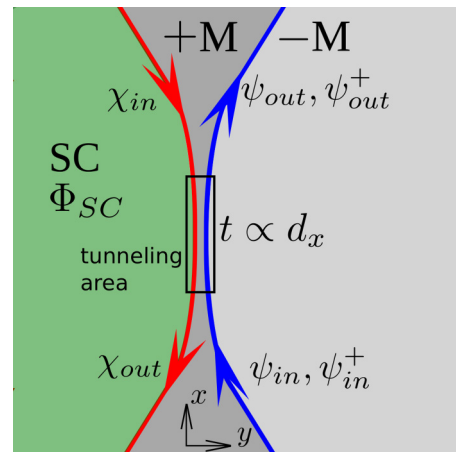

FIG. 7. Structure of the tunneling contact implemented as a constriction of the magnetic material marked as dark gray. The area of hybridization between the wave functions of the counterpropagating neutral and charged chiral channels is indicated by a bar.

The amplitude of the dominant process of normal reflection is given by $1/(1+\lambda)$. The scattering to the Majorana channel scales as $\sim\sqrt{\lambda}$, whereas the Andreev reflection amplitude has the lowest amplitude $\sim\lambda$.

B. Current-phase relation in the tunneling regime

Using the scattering matrix S_t calculated above (21), we obtain the following results for the spectral current and the CΦR (for details see Appendix B):

$$J_\varepsilon(\Phi,\phi_{AB}) = \frac{-4\lambda^3 \sin\Phi \, \sin\varphi_\varepsilon}{((1+\lambda^2)\cos\varphi_\varepsilon + \cos\phi_{AB} - \lambda^2\cos\Phi)^2 + 4\lambda^2\sin^2\varphi_\varepsilon}, \tag{23}$$

$$j(\Phi,\phi_{AB}) = 4\pi\frac{ek_BT}{\hbar}\lambda^2\sin\Phi\sum_{n=0}^{\infty}\frac{1}{(1+\lambda^2)\cosh\left(\frac{\pi k_BT(2n+1)}{E_T}\right) + 2\lambda\,\sinh\left(\frac{\pi k_BT(2n+1)}{E_T}\right) + \cos\phi_{AB} - \lambda^2\cos\Phi}. \tag{24}$$

Here the Thouless energy is given by $E_T = \hbar v/(2L)$. From the CΦR in (24) we see that at high temperatures, $T \gg E_T$, only $n = 0$ term contributes to the sum (24). In this limit we observe a sinusoidal CΦR and the critical current j_c is exponentially suppressed:

$$j(\Phi) \approx \frac{4\pi ek_BT\lambda^2}{\hbar(1+\lambda)^2}\exp(-\pi k_BT/E_T)\sin\Phi. \tag{25}$$

The factor $\frac{\lambda^2}{(1+\lambda)^2}$ is proportional to the full transparency of the junction being the product of the transparencies of the left and the right contacts. This result is similar to the CΦRs for a conventional S/N/S junction with the N region being a long quantum wire [24–26].

In the low temperature regime, $T \ll E_T$, the CΦR is no longer sinusoidal and the critical current $j_c \sim E_T$ decays as $1/L$. Flux dependent oscillations of j_c are sharper compared to those in the transparent regime. The resonant shape of the non-Fraunhofer h/e-periodic modulation is shown in Fig. 9 for weak tunneling $\lambda = 0.1$. The shift of the maximum of j_c by π results from the presence of the Berry phase.

C. Formal continuation of the tunneling solution to the regime of finite transparency

The solution for the scattering matrix (21) follows formally from the tunneling Hamiltonian (20) at any value of t (see Appendix A). Yet, it is only physically justified for $t/v \ll 1$, or $\lambda \ll 1$. We ask ourselves what happens if we extend (21), formally, to an arbitrary value of t/v in the tunneling Hamiltonian (20) and consider the scattering matrix (21) at any value of $\lambda = \tan^2(t/\sqrt{2}v)$. We observe that at $\lambda = 1$ the CΦR obtained for the transparent regime (18) is recovered (up to the geometry dependent phase α). In other words, transparent contacts formed by Y junctions correspond to the intermediate strength $\lambda = 1$ of tunnel contacts, rather than to the regime $\lambda \to \infty$.

In this subsection we investigate the CΦR and the density of states in the N region at arbitrary λ. In particular, we analyze the regime of full transparency, $\lambda \to \infty$, where the scattering matrix S_t reaches the unitary limit and corresponds to the full Andreev reflection in the Dirac channel.

Note that the relation between λ and t/v, obtained in Appendix A, assumes a certain microscopic structure of the contacts and, thus, could also be different. We discuss this in more details in Appendix A.

1. Critical current and CΦRs

As mentioned above, the formal result for CΦR for the tunneling regime (24) is identical to that for the transparent regime (18) at $\lambda = 1$, up to geometry dependent phase α. In Figs. 8 and 9 we illustrate the evolution of CΦRs and critical currents j_c upon increase of the transparency parameter λ. We plot the results at small $\lambda = 0.36$, related to tunneling approximation, and their continuation to higher $\lambda = 4$ and 25.

In the limit $\lambda \to \infty$ the scattering matrix S_t (21) reaches the unitary limit

$$S_t(\lambda \to \infty) = \begin{bmatrix} 0 & 0 & e^{-i\Phi_{SC}} \\ 0 & -1 & 0 \\ e^{i\Phi_{SC}} & 0 & 0 \end{bmatrix}.$$

This matrix describes the process of full Andreev reflection, where an electron converts into a hole with a phase shift of wave function equal to the phase of the SC electrode. At $T = 0$ and $\lambda \to \infty$, where j_c is independent on ϕ_{AB}, the CΦR (24)
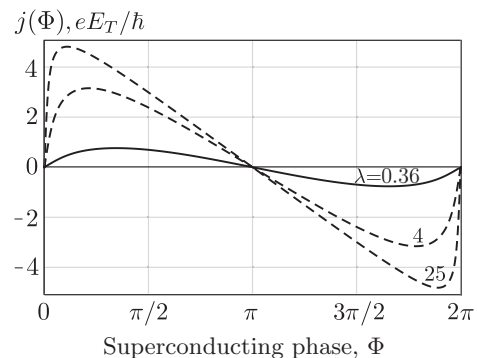

FIG. 8. Bold curve: CΦR found in (24) for tunnel junction at dimensionless tunneling strengths $\lambda = 0.36$. Dashed curves: continuation of the results for CΦR (24) to finite transparencies $\lambda = 4$ and $\lambda = 25$. The current $j(\Phi)$ is measured in units of the Thouless energy E_T with Aharonov-Bohm phase $\phi_{AB} = \pi$ ($\phi_{ext} = 0$) and at low temperature $T = 0.01E_T$. The $\lambda = 25$ curve indicates the tendency to the formation of spikes at unusual even phases $2\pi n$.
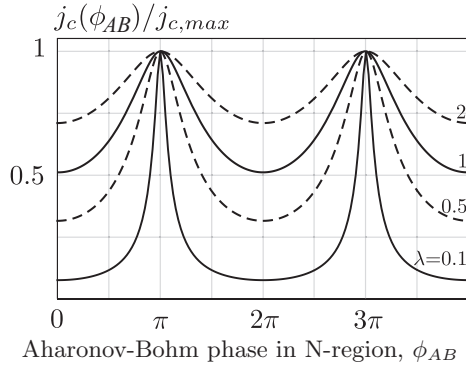
FIG. 9. Dimensionless critical current $j_c(\phi_{AB})/j_{c,\text{max}}$ of the tunnel ($\lambda = 0.1$) and transparent at ($\lambda = 1$ and $4\alpha = \pi$) junctions as a function of Aharonov-Bohm phase $\phi_{AB} = 2\pi f/(h/e)$. Maximum of the critical current is shifted due to the presence of Berry phase. Dashed curves correspond to results at finite $\lambda = 0.5, 2$ found from the tunneling approach. All figures are plotted at low temperature $T = 0.01 E_T$.

shows a sawtooth shape with spikes at *even* phases

$$j(\Phi) = 4\frac{e}{\hbar}E_T \arctan \cot \frac{\Phi}{2}$$

$$= 2\frac{e}{\hbar}E_T(\pi - \Phi) \quad \text{for } 0 < \Phi < 2\pi. \quad (26)$$

In conventional ballistic spinful 1D S/N/S junctions the CΦRs are known to be sawtoothlike [27]. In contrast to our

result (26) the spikes are usually *odd* $\pi + 2\pi n$ and the slope is positive. This difference follows from an additional phase of π acquired by a fermion in a spinful junction after two Andreev reflections from the contacts. For spinful systems, full Andreev reflection is associated with the time-reversal transformation $i\sigma_y K$ of the fermion wave function. Being reflected two times from the left and right contacts, the spinful fermion gets a π phase. In spinless junction under consideration this phase is zero.

2. Density of states

We calculate density of states at arbitrary λ in a branch with the use of ψ_a from (B8) derived in Appendix B. The density of states in chiral Dirac modes are "halves" of the spectral current, because $J_\varepsilon = ev(\rho_\varepsilon^{(a)} - \rho_\varepsilon^{(b)})$ if incoming Majorana fermion modes $\chi_{r,l}$ are not correlated. We introduce the local retarded Green function (calculated at an arbitrary coordinate x in the a branch) as

$$G^{(a)}(t,t') = -i\theta(t-t')\langle\{\psi_a(x,t),\psi_a^+(x,t')\}\rangle.$$

The Fourier transform of this function,

$$G_\varepsilon^{(a)} = \int \langle\{\psi_{a,\omega},\psi_{a,\omega}^+\}\rangle \frac{d\omega}{\varepsilon - \omega + io},$$

gives for the density of states

$$\rho_\varepsilon^{(a)} = -\frac{1}{\pi}\text{Im}G_\varepsilon = \langle\{\psi_{a,\varepsilon},\psi_{a,\varepsilon}^+\}\rangle.$$

Assuming the density of states of χMM in the SC gap is constant, i.e., $\langle\{\chi_{i,-\varepsilon},\chi_{i,\varepsilon}\}\rangle = v^{-1}$, we obtain

$$\rho_\varepsilon^{(a)}(\Phi,\phi_{AB}) = v^{-1}\frac{2\lambda(1 + \lambda^2 + \cos(\phi_{AB} - \varphi_\varepsilon) - \lambda^2\cos(\Phi + \varphi_\varepsilon))}{((1 + \lambda^2)\cos\varphi_\varepsilon + \cos\phi_{AB} - \lambda^2\cos\Phi)^2 + 4\lambda^2\sin^2\varphi_\varepsilon}. \quad (27)$$

In Fig. 10 we plot the density of states $\rho_\varepsilon^{(a)}$ at three values of dimensionless tunneling parameter λ. At weak tunneling, $\lambda = 0.3$ [see Fig. 10(a)], the maxima of $\rho_\varepsilon^{(a)}$ are slightly dependent on Φ. Horizontal lines resemble smeared mesoscopic levels
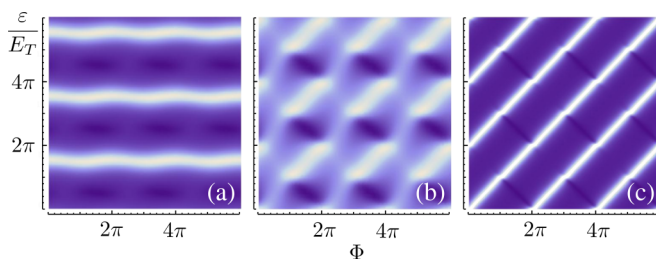

FIG. 10. Spectral density of states (27) of the right movers, $\rho_\varepsilon^{(a)}(\Phi,\varepsilon)$, in the upper a arm of the junction. The energy ε is counted in units of Thouless energy E_T. Blue and white colors correspond to low and high densities, respectively. (a) Weak tunneling regime, $\lambda = 0.3$; the horizontal lines are reminiscent of the quantized levels of the isolated N region; (b) intermediate transparency, $\lambda = 1$; the results coincide with those for a transparent junction at $\alpha = \pi/4$; (c) the case $\lambda = 5$ illustrates the continuation to the high transparency limit (full Andreev reflection), where bright narrow lines are half of full set of smeared Andreev levels. Aharonov-Bohm phase $\phi_{AB} = -\pi/2$ for all three plots.

of an isolated 1D Dirac wire of length L. These maxima can be shifted vertically by a flux induced Aharonov-Bohm phase ϕ_{AB}, because their position is given by

$$\varepsilon_n = (2\pi n - \pi - \phi_{AB})E_T.$$

The result for the intermediate transparency $\lambda = 1$, equivalent to the transparent junction, is shown in Fig. 10(b). We see that the density of states is strongly smeared in this case.

The continuation of $\rho_\varepsilon^{(a)}$ to high transparency ($\lambda \gg 1$) shows that the spectral density is given by 2π-periodic narrow lines of Andreev levels. Their structure can be found from the singularities of (27) at $\lambda \to \infty$ as

$$\varepsilon_n^A = \pm E_T(\Phi + 2\pi n). \quad (28)$$

In Fig. 10(c) we plot the density of states at $\lambda = 5$ which consists of half of the full set of smeared Andreev levels (28). Note that level positions are independent of the Aharonov-Bohm phase. This follows from the fact that the electron and the reflected hole get opposite Aharonov-Bohm phases, which compensate each other in closed paths.

3. Persistent current at $\Phi = 0$

Both Dirac channels carry large electric currents. The difference of this currents leads to the net electric current $j(\Phi,\phi_{AB})$ calculated above. If the superconducting phase

difference vanishes, $\Phi = 0$, the currents in the Dirac channels are equal $j_a = j_b \equiv j_p$ and, thus, cancel each other. In this case $j_p(\phi_{AB})$ is the persistent loop current which we calculate in this subsection. We obtain

$$j_p(\phi_{AB}) = \int \frac{1}{2}\left(1 - \tanh \frac{\varepsilon}{2T}\right)\rho_\varepsilon^{(a)}(\Phi = 0, \phi_{AB})d\varepsilon. \quad (29)$$

The result of the integration consists of two parts:

$$j_p(\phi_{AB}) = j_{p,0} + \delta j_p(\phi_{AB}). \quad (30)$$

$$\delta j_p(\phi_{AB}) = 2\pi \, \sin\phi_{AB} \frac{k_B e}{\hbar} T \sum_{n=0} \frac{1}{(1 + \lambda^2)\cosh\left(\frac{\pi T(2n+1)}{E_T}\right) + 2\lambda \, \sinh\left(\frac{\pi T(2n+1)}{E_T}\right) + \cos\phi_{AB} - \lambda^2}. \quad (31)$$

At high temperatures, $T \gg E_T$, the oscillating part $\delta j_p(\phi_{AB})$ is sinusoidal. Its amplitude is exponentially suppressed and, moreover, in the limit of fully transmitted contacts $\lambda \gg 1$ it decays as λ^{-2}:

$$\delta j_p(\phi_{AB}) = 4\pi \frac{k_B e}{\hbar(1 + \lambda)^2} T \, \exp(-\pi k_B T/E_T)\sin\phi_{AB}. \quad (32)$$

At low temperatures, $T \ll E_T$, and in the weak tunneling limit $\lambda \ll 1$ we obtain a sawtoothlike shape:

$$\delta j_p(\phi_{AB}) = 2\frac{e}{\hbar}E_T \arctan \tan \frac{\phi_{AB}}{2}. \quad (33)$$

The result for the persistent current as the function of ϕ_{AB} in this poorly transmitting regime looks like dual to the result for sawtooth CΦR in the fully transmitting limit (26). Values of oscillations amplitudes of j_c and δj_p have maximum at $\lambda \gg 1$ and $\lambda \ll 1$, respectively. The difference between (33) and (26) is in opposite signs of the slopes of these sawtooth characteristics. Spikes in $\delta j_p(\phi_{AB})$ are related to crossings between quantized resonant levels and Fermi energy. In the expression (33) these spikes hold for odd Aharonov-Bohm phases of $(2n + 1)\pi$ but in general case the zero point of ϕ_{AB} is ill defined due to the presence of magnets in setups.

The low-T result for $\delta j_p(\phi_{AB})$ (up to zero phase shift) for the transparent interferometer (Fig. 3) is formally given by (31) at $\lambda = 1$. We get $\delta j_p(\phi_{AB})$ dependence in this case, dual to CΦR (19), with opposite signs of the slopes and infinite derivatives at odd Aharonov-Bohm phases

$$\delta j_p(\phi_{AB}) = \frac{e}{\hbar}E_T \frac{\sin(\phi_{AB})\ln\left(\cos^2\left(\frac{\phi_{AB}}{2}\right)\right)}{\cos(\phi_{AB}) - 1}. \quad (34)$$

We recall that chiral Dirac edge modes are spatially separated in our devices and Andreev pairs are nonlocal. External magnetic flux f enclosed by the perimeter of the interferometer induce single-electron Aharonov-Bohm phase $2\pi f/(h/e)$ in the Dirac channels. This results in fractional $2\Phi_0$ periodicity of the critical and persistent currents.

V. SCATTERING IN TERMS OF MAJORANA MODES

One can describe the scattering between the Dirac and Majorana chiral modes by representing the ψ operators in the N channel with the help of two auxiliary charged-neutral Majorana operators γ_1 and γ_2. These modes do not carry charge

The first part, $j_{p,0}$, originates from the unity in the factor $(1 - \tanh \frac{\varepsilon}{2T})$ in the integral (29). This part describes a large equilibrium current carried by chiral Dirac modes around a magnetic domain surrounded by the area of opposite magnetization. This current is independent of ϕ_{AB} and is estimated as $j_{p,0} \sim (e/\hbar)M$.

The second part $\delta j_p(\phi_{AB})$ in (30) is of our interest. This part is sensitive to the presence of superconducting contacts and to the interference due to Andreev reflections. It is thus periodic in ϕ_{AB} but it is much smaller than $j_{p,0}$. We find

separately but their superpositions do. The different SC phases of the opposite contacts result in a fusion of the auxiliary γ_1 and γ_2 modes, which is responsible for a Cooper pair transfer from one lead to the other.

In this section we discuss the scattering in the Majorana basis for the tunneling and transparent contacts. We analyze in detail the regime $\lambda = 1$ (keeping α as a free parameter), since it corresponds to the case of the transparent junction (18) up to geometry dependent α and the Berry phases.

The Majorana basis is defined through the following transformation for both the left and the right contacts:

$$\psi_i = \frac{1}{\sqrt{2}}(\gamma_{1,i} + i\gamma_{2,i})e^{-i\Phi_{SC}/2}, \quad (35)$$

where the index i here stands for *in* and *out* channels. The S_t matrix (21) under this transformation at arbitrary λ reads

$$\begin{bmatrix} \gamma_{1,\text{out}} \\ \chi_\text{out} \\ \gamma_{2,\text{out}} \end{bmatrix} = \begin{bmatrix} 1 & 0 & 0 \\ 0 & \frac{1-\lambda}{1+\lambda} & -\frac{2\sqrt{\lambda}}{1+\lambda} \\ 0 & \frac{2\sqrt{\lambda}}{1+\lambda} & \frac{1-\lambda}{1+\lambda} \end{bmatrix} \begin{bmatrix} \gamma_{1,\text{in}} \\ \chi_\text{in} \\ \gamma_{2,\text{in}} \end{bmatrix}. \quad (36)$$

According to (36) γ_1 mode is always fully decoupled, consistent with the scattering theory of Li, Fleury, and Büttiker [17]. In the weak tunneling limit $\lambda \ll 1$ the modes χ and γ_2 scatter into each other with the amplitude $\sim\sqrt{\lambda}$. In the opposite unitary limit $\lambda \to \infty$ all modes are decoupled from each other but both χ and γ_2 invert signs meaning that the corresponding Dirac fermions experience the full Andreev reflection. In the intermediate case $\lambda = 1$ (Fig. 11, left) the modes χ and γ_2 fully convert into each other: $\gamma_{2,\text{out}} = \chi_\text{in}$ and $\chi_\text{out} = -\gamma_{2,in}$.

The presence of the scattering phase α in the scattering matrix (12) of the transparent Dirac-Majorana contacts changes the situations considerably. We apply again the transformation (35) to ψ operators and obtain the following S matrix in the Majorana basis (setting $d = 0$)

$$\begin{bmatrix} \gamma_{1,\text{out}} \\ \chi_\text{out} \\ \gamma_{2,\text{out}} \end{bmatrix} = \begin{bmatrix} \cos^2\alpha & -\sin\alpha & -\frac{\sin 2\alpha}{2} \\ -\sin\alpha & 0 & -\cos\alpha \\ \frac{\sin 2\alpha}{2} & \cos\alpha & -\sin^2\alpha \end{bmatrix} \begin{bmatrix} \gamma_{1,\text{in}} \\ \chi_\text{in} \\ \gamma_{2,\text{in}} \end{bmatrix}. \quad (37)$$

This matrix coincides with that of (36) in the limit $\lambda = 1$ only if $\alpha = 0$. For the other values of α all the modes are mixing with each other. At arbitrary α there is mixing between all of the modes except for χ_in and χ_out. Mixing between χ_in and
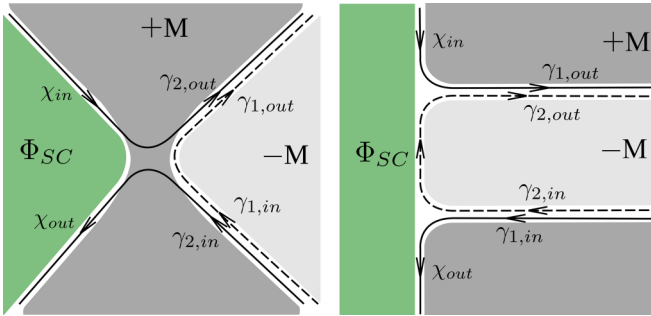
FIG. 11. Scattering in normal Dirac ψ, ψ^+ and neutral-charge channels χ written in terms of auxiliary Majorana modes γ_1, γ_2. Left: tunnel contact described by S_t matrix (21) at $\lambda = 1$. Right: transparent contact described by S matrix (12) at $\alpha = \pm\pi/2$.

χ_{out} is possible if we a add second contact with a different SC phase. We illustrate the scattering in the particular case of $\alpha = \pm\pi/2$ in Fig. 11 (right), where the incoming χ mode converts into γ_1 mode and vice versa. Note that, in this case, γ_2 mode is not converted to the others but gets an inversion of the sign, $\gamma_{2,\text{out}} = -\gamma_{2,\text{in}}$.

VI. SUMMARY

To conclude, we analyzed two limits of 1D long ballistic Josephson junctions where the leads are formed by gapless 1D chiral Majorana channels. These junctions can be realized as hybrid structures involving 3D topological insulator surface in proximity with s-wave superconducting electrodes and magnetic materials. More generally, our model describes transport of Cooper pairs between 2D topological superconductors supporting neutral edge modes. The normal region of these setups is formed by two chiral Dirac modes spaced by a magnetic material. Such a normal part is effectively spinless because the spin textures are locked to profiles of magnetic domain walls.

In the first part of the work we have calculated the CΦR in the regime of high transparency. In this limit the left and the right contacts of the junction consist each of two Dirac-Majorana converters built by magnet/superconductor interfaces. We find that this system has a continuous spectral current, a 2π-periodic nonsinusoidal CΦR at low temperatures, and an h/e-periodic dependence of the critical current on the magnetic flux. The critical current amplitude at zero temperature is given by Thouless energy which is proportional to inverse dwell time of the normal region. The junction can act as a SQUID because the two Dirac channels are spatially separated. An Andreev pair in this case appears to be spatially nonlocal, which offers a possibility of inducing an internal Aharonov-Bohm phase. This leads to one of our central results: the critical current and the persistent current in the normal region show fractional h/e-periodic patterns.

In the second part of the work we have studied another realization of the junction where Dirac and Majorana channels are coupled through a tunnel barrier. The CΦR of such a tunnel junction was found in terms of the tunneling Hamiltonian approach and corresponding scattering matrix. The resulting critical current patterns show sharper resonant peaks as

compared to those for the transparent junction. We have also studied the formal extension of the tunneling solution to the high transparency regime and compared it with the one obtained in the first part of the work.

Alternative Josephson junctions with spatially separated Andreev channels were proposed in Refs. [22,23]. In these systems the normal part between the superconductors is a quantum Hall bar and the current is carried by the chiral edge states. We compare our system with those based on quantum Hall junctions. (i) In our system the low-T critical current scales as $1/\mathcal{L}$, where $\mathcal{L}$ is the perimeter of the normal part of the junction. In contrast in the closest counterpart of our system, i.e., in the spinless quantum Hall setup, the low-T critical current scales as $1/\mathcal{L}^3$. In the spinful quantum Hall junction the critical current also scales as $1/\mathcal{L}$. (ii) In our system the CΦR is strongly nonsinusoidal and may have infinite derivatives or discontinuities at even values of the phase. This feature may be associated with the presence of a gapless sector of excitations in 1D Majorana channels. In contrast, in the spinless quantum Hall junction CΦR is exactly sinusoidal. The CΦRs of the spinful quantum Hall junction are nonsinusoidal as well; however, only odd discontinuities are possible.

Interferometers involving chiral Majorana modes [14–18] could find their applications as measuring devices of topological qubits [15]. In this paper we have explored a dual setup, in which the equilibrium Josephson current is carried by interfering chiral Dirac electrons between chiral Majorana leads. Embedded into schemes with vortices and/or magnetic or SC islands supporting zero-energy Majorana pairs, a Josephson based quantum interferometer might be of advantage, e.g., for performing quantum readout of topological qubits.

APPENDIX A: DERIVATION OF THE SCATTERING MATRIX OF A TUNNEL CONTACT

The local form of tunneling Hamiltonians (20) is an approximation, because, microscopically, such contacts are formed by constrictions of finite size as depicted in Fig. 7. If the constriction is wide and the hybridization is negligible, the parallel chiral channels along SC/+M and +M/−M junctions have opposite (orthogonal) spin textures. In the tunneling area, shown as the constriction of the magnetic material in the black bar, the eigenfunctions can be approximated by superpositions of the eigenfunctions of the isolated Dirac and Majorana channels, $\xi^{(e)}$, $\xi^{(h)}$, and $\xi^{(M)}$. This means that an electron coming into the tunneling area starts to oscillate between hole- and Majorana-like states with a rate, proportional to a hybridization of the channels, estimated as $M e^{-M d_y}$, where

d_y is a transversal constriction length. Finally, the incoming electron scatters into a superposition of outgoing electron, hole, and neutral excitation in the Majorana channel. From this qualitative picture one can conclude that the scattering matrix should be periodic with respect to the phase of these oscillations, given as a product of hybridization energy and the constriction dwell time $M e^{-M d_y/v} d_x/v$.

Here, we derive this periodic behavior of the S_t matrix from the local tunneling Hamiltonian (20). We employ the Heisenberg equations of motion

$$\begin{bmatrix} (v\partial_x - \partial_t)\psi(x) \\ (v\partial_x - \partial_t)\chi(-x) \\ (v\partial_x - \partial_t)\psi^+(x) \end{bmatrix} = it\delta(x)\mathcal{T}\begin{bmatrix} \psi(x) \\ \chi(x) \\ \psi^+(x) \end{bmatrix}, \quad \text{(A1)}$$

where the tunnel matrix is given by

$$\mathcal{T} = \begin{bmatrix} 0 & e^{-i\frac{\Phi_{SC}}{2}} & 0 \\ e^{i\frac{\Phi_{SC}}{2}} & 0 & -e^{-i\frac{\Phi_{SC}}{2}} \\ 0 & -e^{i\frac{\Phi_{SC}}{2}} & 0 \end{bmatrix}. \quad \text{(A2)}$$

We write $\chi(-x)$ in these equations in order to make the chirality of the Majorana mode the same as that of the charged channel. In this representation we can consider incoming and outgoing states as those at $x < 0$ and at $x > 0$, respectively.

It follows from the x integration of (A1), (A2) around the point of contact $x = 0$ that the relation between the tunneling matrix $\mathcal{T}$ and the scattering matrix S_t reads

$$S_t = \exp[i(t/v)\mathcal{T}]. \quad \text{(A3)}$$

Calculating the exponent we obtain

$$S_t = \begin{bmatrix} \frac{1}{1+\lambda} & \frac{i\sqrt{2\lambda}}{1+\lambda}e^{-i\frac{\Phi_{SC}}{2}} & \frac{\lambda}{1+\lambda}e^{-i\Phi_{SC}} \\ \frac{i\sqrt{2\lambda}}{1+\lambda}e^{i\frac{\Phi_{SC}}{2}} & \frac{1-\lambda}{1+\lambda} & \frac{-i\sqrt{2\lambda}}{1+\lambda}e^{-i\frac{\Phi_{SC}}{2}} \\ \frac{\lambda}{1+\lambda}e^{i\Phi_{SC}} & \frac{-i\sqrt{2\lambda}}{1+\lambda}e^{i\frac{\Phi_{SC}}{2}} & \frac{1}{1+\lambda} \end{bmatrix}, \quad \text{(A4)}$$

where the dimensionless tunneling strength $\lambda(t)$ is given by

$$\lambda(t) = \tan^2\frac{t}{\sqrt{2}v}. \quad \text{(A5)}$$

This tunneling S_t matrix is unitary and obeys the particle-hole symmetry $S_t(\varepsilon) = \mathcal{Z}S_t^*(-\varepsilon)\mathcal{Z}$ like S. The eigenvalues of (A4) are given by $e^{i\sqrt{2}t/v}$; $e^{-i\sqrt{2}t/v}$; 1.

The solution method leading to (A4) and (A5) is not universally accepted. Rather, a different ansatz was used in various problems on transport in 1D systems such as tunneling between edge states of QHE [28], impurity scattering in Luttinger liquid at $g = 1/2$ [29], or resonant Andreev reflection from zero-mode Majorana bound state [30]. Following these works we should have taken the local ψ and χ operators at point $x = 0$ as

$$\psi = \frac{\psi(-0) + \psi(+0)}{2}, \quad \chi = \frac{\chi(-0) + \chi(+0)}{2}. \quad \text{(A6)}$$

Relations (A6) produce then the same solution for the scattering matrix as in (A4). However, the parameter λ is now different and is given by

$$\tilde{\lambda}(t) = \frac{t^2}{2v^2}. \quad \text{(A7)}$$

The two solutions coincide in the weak coupling limit $t/v \ll 1$. For larger values of t the difference is substantial. For instance, the unitary limit $\tilde{\lambda} \to \infty$ is achieved with (A6) and (A7) at $t \to \infty$. In contrast, with (A3) it is reached at $t_n = \sqrt{2}(\pi/2 + \pi n)v$.

We conjecture that the solution method, leading to (A3), applies if the constriction is smooth enough, so that the validity of the low energy description provided by (1) and (20) is not violated in any point of the constriction. Then, Eq. (A1) is solved as a regular differential equation. On the other hand, the ansatz (A6) is probably applicable for sharp enough constrictions. This ambiguity should be resolved by solving 2D BdG equations for the constriction geometry.

APPENDIX B: DERIVATION OF CΦR IN THE TUNNELING REGIME

In this appendix we present technical details of the calculation of the Josephson current. We find the CΦR as the difference between the chiral currents in a and b arms by using the tunnel junction scattering matrix S_t, given by (A4). We take the first and the third lines of (A4), disregarding the outgoing Majorana field χ_{out} (line 2), and obtain

$$\begin{bmatrix} \psi_{out,\varepsilon} \\ \psi_{out,-\varepsilon}^+ \end{bmatrix} = \begin{bmatrix} \frac{1}{1+\lambda} & \frac{\lambda e^{-i\Phi_{SC}}}{1+\lambda} \\ \frac{\lambda e^{i\Phi_{SC}}}{1+\lambda} & \frac{1}{1+\lambda} \end{bmatrix}\begin{bmatrix} \psi_{in,\varepsilon} \\ \psi_{in,-\varepsilon}^+ \end{bmatrix} + \frac{i\sqrt{2\lambda}}{1+\lambda}\chi_{in,\varepsilon}\begin{bmatrix} e^{-i\frac{\Phi_{SC}}{2}} \\ -e^{i\frac{\Phi_{SC}}{2}} \end{bmatrix}. \quad \text{(B1)}$$

The matrix in the right hand side of Eq. (B1) contains amplitudes of normal and Andreev reflection, while the last term describes coupling with the equilibrium Majorana *in* channel. This term is responsible for the spectral current (23) being continuous, due to the gapless spectrum of the incoming lead Majorana mode.

To proceed we rewrite Eq. (B1) as follows:

$$\begin{bmatrix} \psi_{out,\varepsilon} \\ \psi_{in,-\varepsilon}^+ \end{bmatrix} = \mathcal{M}_{\Phi_{SC}}\begin{bmatrix} \psi_{out,-\varepsilon}^+ \\ \psi_{in,\varepsilon} \end{bmatrix} + i\sqrt{2\lambda}\chi_{in,\varepsilon}\begin{bmatrix} e^{i\frac{\Phi_{SC}}{2}} \\ e^{-i\frac{\Phi_{SC}}{2}} \end{bmatrix}. \quad \text{(B2)}$$

The matrix $\mathcal{M}_{\Phi_{SC}}$ in (B2) is given by

$$\mathcal{M}_{\Phi_{SC}} = \begin{bmatrix} \lambda e^{i\Phi_{SC}} & 1-\lambda \\ 1+\lambda & -\lambda e^{-i\Phi_{SC}} \end{bmatrix}.$$

Using (B2) we formulate the boundary conditions for the left and right contacts. We introduce the field $\Psi_{\varepsilon,x} = [\psi_{a,\varepsilon}, \psi_{b,-\varepsilon}^+, \psi_{a,-\varepsilon}^+, \psi_{b,\varepsilon}]_x^T$, which depends on ε and on the coordinate x along the Dirac channels. Indices a and b stand for the upper and lower Dirac modes (see Fig. 6). We start from the left contact where $\Phi_{SC} = \Phi/2$ and $x = -L/2$. Using (B2) and its Hermitian conjugate at $\varepsilon \to -\varepsilon$ as well as the property of the real Majorana field, $\chi_{l,-\varepsilon}^+ = \chi_{l,\varepsilon}$, we derive

$$\begin{bmatrix} \gamma_0 & -\mathcal{M}_{\Phi/2} \\ -\mathcal{M}_{\Phi/2}^* & \gamma_0 \end{bmatrix}\Psi_{\varepsilon,-L/2} = i\sqrt{2\lambda}\eta_{\Phi/2}\chi_{l,\varepsilon}. \quad \text{(B3)}$$

Here γ_0 is the 2×2 identity matrix in the left upper block and $\eta_{\Phi/2} = [e^{i\frac{\Phi}{4}}, e^{-i\frac{\Phi}{4}}, -e^{-i\frac{\Phi}{4}}, -e^{i\frac{\Phi}{4}}]^T$. Note that for the left contact b components of $\Psi_{\varepsilon,-L/2}$ are *in* fields, while a components are *out* fields: $\psi_{a,-L/2} = \psi_{out}$ and $\psi_{b,-L/2} = \psi_{in}$. The rank of the 4×4 matrix in (B3) equals 2 and the eigenvalues

are equal to $0,0,2,2$ regardless of the values of λ and Φ. The condition for the right contact is obtained from (B3) by the replacements

$$\Phi \to -\Phi, \quad \chi_l \to \chi_r, \quad \Psi_{\varepsilon,-L/2} \to s_x \gamma_x \Psi_{\varepsilon,L/2}. \quad \text{(B4)}$$

The Pauli matrix s_x, introduced in (B4), mixes the 2×2 blocks in (B3) acting as a particle-hole transformation, while γ_x acts inside of the blocks. The product $s_x \gamma_x$ interchanges a and b indices in $\Psi_{\varepsilon,x}$. We find that the fields in the middle of N region, $\Psi_{\varepsilon,0} \equiv \Psi_{\varepsilon,x=0}$, can be expressed via the operators at the ends of the Dirac channels, $\Psi_{\varepsilon,-L/2}$ and $\Psi_{\varepsilon,L/2}$, using the dynamical and geometrical phases:

$$\Psi_{\varepsilon,-L/2} = \mathcal{D}_\varepsilon \mathcal{F} \Psi_{\varepsilon,0}, \quad \text{(B5)}$$

$$\Psi_{\varepsilon,L/2} = s_x \gamma_x \mathcal{D}_\varepsilon \mathcal{F} s_x \gamma_x \Psi_{\varepsilon,0}. \quad \text{(B6)}$$

Here $\mathcal{D}_\varepsilon = \mathrm{diag}[e^{-i\varphi_\varepsilon/4}, e^{i\varphi_\varepsilon/4}, e^{-i\varphi_\varepsilon/4}, e^{i\varphi_\varepsilon/4}]$ and $\mathcal{F} = \mathrm{diag}[e^{-i\phi_{\mathrm{ext}}/4}, e^{-i\phi_{\mathrm{ext}}/4}, e^{i\phi_{\mathrm{ext}}/4}, e^{i\phi_{\mathrm{ext}}/4}]$. The external phase ϕ_{ext} is equal to the sum of Aharonov-Bohm and Berry phases and the dynamical phase φ_ε accumulated an electron of energy ε or a hole of energy $-\varepsilon$, enclosing the interference loop of the length $2L$. Here

$$\varphi_\varepsilon = \frac{\varepsilon}{E_T}, \quad E_T = \frac{\hbar v}{2L}. \quad \text{(B7)}$$

The relations (B3), (B4) together with (B5), (B6) make the problem of finding the four components of $\Psi_\varepsilon(0)$ algebraically close. The result for the first component reads

$$\psi_{a,\varepsilon} = \sqrt{2\lambda}\, e^{-i\frac{\Phi+\varphi_\varepsilon+\phi_{\mathrm{ext}}}{4}} \frac{e^{i\frac{\varphi_\varepsilon}{2}} \left(e^{i\frac{\phi_{\mathrm{ext}}+\Phi}{2}} \sin\frac{\phi_{\mathrm{ext}}-\varphi_\varepsilon}{2} - \lambda \sin\frac{\Phi+\varphi_\varepsilon}{2}\right) \chi_{l,\varepsilon} + \left(\sin\frac{\phi_{\mathrm{ext}}-\varphi_\varepsilon}{2} + \lambda e^{i\frac{\phi_{\mathrm{ext}}+\Phi}{2}} \sin\frac{\Phi+\varphi_\varepsilon}{2}\right) \chi_{r,\varepsilon}}{(1+\lambda^2)\cos\varphi_\varepsilon - \cos\phi_{\mathrm{ext}} - \lambda^2 \cos\Phi + 2i\lambda \sin\varphi_\varepsilon}. \quad \text{(B8)}$$

The Dirac field in the b channel is obtained using the geometrical symmetry of the setup and is given by

$$\psi_{b,\varepsilon}(\Phi, \chi_r, \chi_l) = \psi_{a,\varepsilon}(-\Phi, \chi_l, \chi_r). \quad \text{(B9)}$$

The operator relations (B8) and (B9) are used to calculate

$$j = j_a - j_b = -ev \int (\langle \psi_{a,\varepsilon}^+ \psi_{a,\varepsilon} \rangle - \langle \psi_{b,\varepsilon}^+ \psi_{b,\varepsilon} \rangle) d\varepsilon,$$

which results in the CΦR presented in (24).

[1] J. Alicea, Rep. Prog. Phys. **75**, 076501 (2012).
[2] C. Nayak, S. H. Simon, A. Stern, M. Freedman, and S. Das Sarma, Rev. Mod. Phys. **80**, 1083 (2008).
[3] A. Yu. Kitaev, Phys. Usp. **44**, 131 (2001).
[4] N. Read and D. Green, Phys. Rev. B **61**, 10267 (2000).
[5] G. Moore and N. Read, Nucl. Phys. B **360**, 362 (1991).
[6] L. Fu and C. L. Kane, Phys. Rev. B **79**, 161408 (2009).
[7] Y. Oreg, G. Refael, and F. von Oppen, Phys. Rev. Lett. **105**, 177002 (2010).
[8] J. Nilsson, A. R. Akhmerov, and C. W. J. Beenakker, Phys. Rev. Lett. **101**, 120403 (2008).
[9] L. Fu and C. L. Kane, Phys. Rev. Lett. **100**, 096407 (2008).
[10] M. Z. Hasan and C. L. Kane, Rev. Mod. Phys. **82**, 3045 (2010).
[11] R. M. Lutchyn, J. D. Sau, and S. Das Sarma, Phys. Rev. Lett. **105**, 077001 (2010).
[12] D. M. Badiane, M. Houzet, and J. S. Meyer, Phys. Rev. Lett. **107**, 177002 (2011).
[13] C. W. J. Beenakker, D. I. Pikulin, T. Hyart, H. Schomerus, and J. P. Dahlhaus, Phys. Rev. Lett. **110**, 017003 (2013).
[14] L. Fu and C. L. Kane, Phys. Rev. Lett. **102**, 216403 (2009).
[15] A. R. Akhmerov, J. Nilsson, and C. W. J. Beenakker, Phys. Rev. Lett. **102**, 216404 (2009).
[16] K. T. Law, P. A. Lee, and T. K. Ng, Phys. Rev. Lett. **103**, 237001 (2009).
[17] J. Li, G. Fleury, and M. Büttiker, Phys. Rev. B **85**, 125440 (2012).
[18] G. Strubi, W. Belzig, M. S. Choi, and C. Bruder, Phys. Rev. Lett. **107**, 136403 (2011).
[19] L. Jiang, D. Pekker, J. Alicea, G. Refael, Y. Oreg, and F. von Oppen, Phys. Rev. Lett. **107**, 236401 (2011).
[20] S.-P. Lee, K. Michaeli, J. Alicea, and A. Yacoby, Phys. Rev. Lett. **113**, 197001 (2014).
[21] G. Tkachov, P. Burset, B. Trauzettel, and E. M. Hankiewicz, Phys. Rev. B **92**, 045408 (2015).
[22] J. A. M. van Ostaay, A. R. Akhmerov, and C. W. J. Beenakker, Phys. Rev. B **83**, 195441 (2011).
[23] A. Yu. Zyuzin, Phys. Rev. B **50**, 323 (1994).
[24] D. L. Maslov, M. Stone, P. M. Goldbart, and D. Loss, Phys. Rev. B **53**, 1548 (1996).
[25] I. O. Kulik, Zh. Eksp. Teor. Fiz. **57**, 1745 (1969) [Sov. Phys. JETP **30**, 944 (1970)].
[26] R. Fazio, F. W. J. Hekking, and A. A. Odintsov, Phys. Rev. B **53**, 6653 (1996).
[27] I. O. Kulik and A. N. Omel'yanchuk, Zh. Eksp. Teor. Fiz. **68**, 2139 (1975) [Sov. Phys. JETP **41**, 1071 (1970)].
[28] C. de C. Chamon, D. E. Freed, and X. G. Wen, Phys. Rev. B **53**, 4033 (1996).
[29] R. Egger and H. Grabert, Phys. Rev. B **58**, 10761 (1998).
[30] L. Fidkowski, J. Alicea, N. H. Lindner, R. M. Lutchyn, and M. P. A. Fisher, Phys. Rev. B **85**, 245121 (2012).